Demonstration of the Use of Bayesian Priors in GHG retrievals from Laser Heterodyne Radiometer Measurements

LASER HETERODYNE RADIOMETRY

HISTORY

Figure A.1. Robert Menzies published a series of papers in 1970s that began the steady growth in LHR research enabled by improving technologies.

Robert Menzies
(1970s)

- "Remote sensing with infra-red heterodyne radiometers", Opto-electronics volume 4, pages179–186 (1972).
- "Remote detection of SO_2 and CO_2 with a heterodyne radiometer", Appl. Phys. Lett. 22, 592 (1973).
- "Laser heterodyne detection techniques." in Laser Monitoring of the Atmosphere, pp 297–353 (1976).

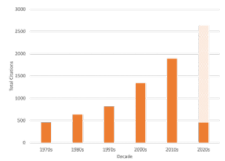

Figure A.2. LHR publications by decade.

THEORY AND PRACTICE

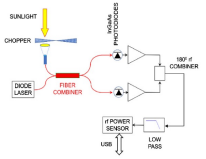

Figure A.3. A schematic of a laser heterodyne system.

- Adapted from and analogous to radio receiver technology.
- Incoming light is combined with light from a narrow-band laser source (the local oscillator or LO) on a photodetector.
- The detector output contains AC electronic signals at the (optical) difference frequencies.
- PHOCS heterodyne signals are proportional to the solar spectrum at the LO wavelength.
- When the LO coincides with an optical absorbance, the heterodyne signal intensity will drop by an amount proportional to the absorbance.

electronic bandwidth of the detection system

The resolution is determined by the electronics bandwidth

- Not an optical element or other physical parameter (dispersing element, optical path difference in FTIR).
- Not the laser linewidth.

Almost always better than FTIR!

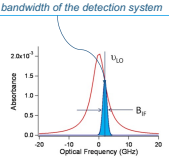

Figure A.4. Illustration of the role of rf bandwidth as a laser is tuned across an absorption line.

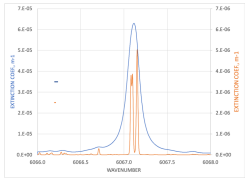

Figure A.5. Simulated extinction coefficient of methane transitions near sea level (blue curve) and in the mid stratosphere. For reference, the small vertical bars show 1 GHz and 200 MHz bandwidths.

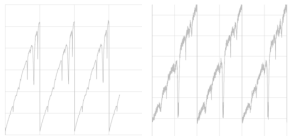

Figure A.6. Traces of several sweeps of a PHOCS instrument in Santa Fe, NM. The left panel shows a region near 1648 nm collected in February 2022 with a 200 MHz BW. The right panel shows the same region collected in May 2022 with a 50 MHz BW. Both spectra show dominant absorption due to methane absorption lines flanked by carbon dioxide features.

PAST AND CURRENT DEPLOYMENTS

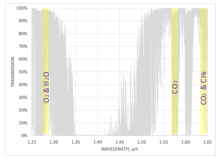

Figure B.1. The near infrared provides an attractive target for atmospheric constituents present at ppm mixing ratios. In addition, weak absorptions ($^1\Delta_g$) of oxygen. We have demonstrated the utility of fitting these transitions in refining estimates of vertical profiles of temperature and pressure.

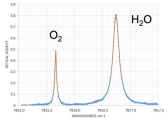

Figure B.3. Observed and fit water and oxygen lines near 1278 nm.

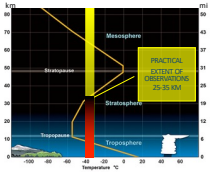

Figure B.2. In practice, as gas density decreases with pressure, most species contributions from above the mid stratosphere are less consequential.

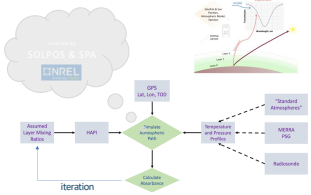

Figure B.4. A schematic of our retrieval process. The PHOCS instrument is equipped with a GPS unit that provides real time location and TOD information. This data is used to model a solar path. The solar simulation code is based on publicly available packages from NREL and NOAA. Additional meta data (specifically temperature and pressure) currently is drawn from statistical analysis of radiosonde data. The use of sensors in commercial aircraft is also being explored.

CURRENT PROJECT STATUS

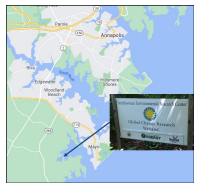

Figure B.5. SERC/GCREW site location. Washington, DC is located ~40 km due west.

Mesa Photonics and GWU are installing 2 GHG instruments at the Smithsonian Environmental Research Center's Global Change Research Wetland. GCREW is a 70-hectare brackish marsh and is home to several long-term experiments designed to explore the impact of sea-level rise on coastal wetland ecosystems and carbon-exchange. A ~2 m diameter, autonomous observatory dome will house both a PHOCS instrument equipped with 3 lasers (centered at ~1278 nm for O_2, H_2O, 1572 for CO_2, and 1651 for CH_4, CO_2, and H_2O) and an upgraded version of an open-path laser absorption instrument previously used to monitor GHGs above thawing permafrost. Also on site are several experiments that record surface concentrations and fluxes for both CO_2 and CH_4. Meteorological data is also collected on site. Additional GHG data is available at a NEON tower, also located at SERC.

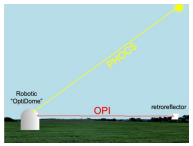

Figure B.6. Schematic of the installation at SERC/GCREW. This location provides year-round, clear sky views with nearly flat horizons.

BAYESIAN PRIORS

For most greenhouse gases (specifically CO_2 and CH_4), prior data to constrain vertical profiles is much sparser than for temperature, pressure, and humidity. Therefore, a different approach to constraining LHR fits is required. The Bayesian paradigm applies prior knowledge and observations to a model being tested. It is the foundation upon which inverse modeling in the atmospheric sciences is built and involves weighting the error to find the optimal value of a state vector given the observations.

Our working assumption is that data collected by our PHOCS instrument at a particular location will provide the best guidance for constraining vertical profiles of GHG mixing ratios at that sensor location. In our retrievals, we assume a 6 layer model for the atmosphere: 0-1 km, 1-2 km, 2-5 km, 5-10 km, 10 – 20 km, >20km. Figure C.1 shows a distribution of observed methane concentrations within those altitude bins, each binned into 200 ppb windows.

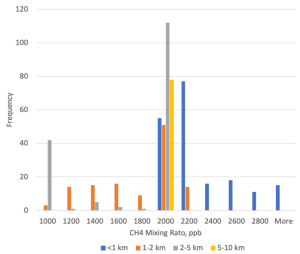

Figure C.1. Survey of methane concentrations at different altitudes in the troposphere spanning many global locations. Most of the measurements here were collected in aircraft campaigns, but additional data from balloon and satellites are also shown.

The Bayesian process begins with a set of hypotheses, here the probability of observing the mixing ratio of a particular GHG at a particular altitude in the atmosphere within a bin of mixing ratio. This is denoted as ***p(H)***. For methane, this might be the probability of observing methane withing a particular 200 ppb wide bin from zero to several 10s of ppm. We might assume that there is equal probability of observing a mixing ratio within each bin or take a set of observations from other observations (such as the distribution shown in Figure C.1). In either case, this set of guessed concentrations in the Bayesian parlance serve as a set of ***priors.***

Once we collect data (specifically, mixing ratios for a GHG at various altitudes as found in fits to the collected spectrum, a distribution, ***p(D)***, *emerges* for each altitude bin. The Bayesian theorem states that we can estimate the probability of some outcome in our hypothesis given the data collected, ***p(H|D)***. This can be given in the following equation, where ***p(D|H)*** is the likelihood of D given H. Further, the ***posterior*** distribution ***p(H|D)*** will serve as the ***priors*** for the next set of observations.

$$p(H|D) = \frac{p(H)\,p(D|H)}{p(D)}$$

This can be illustrated by the following example. Let us assume as our initial priors the distribution of methane mixing ratios in the surface level as given in Figure C.1. Further, let us assume that we perform several observations (i.e., collect and fit PHOCS spectra to find the lowest layer mixing ratio, and that these measurements give results centered at 1.8 ± 0.1 ppm. The initial distribution would predict concentrations this low. However, with just a few measurements, the distribution shifts toward lower levels. Given that several spectra are collected each minute in this instrument, a site–specific distribution is formed that provides both the mixing ratio, but also its uncertainty.

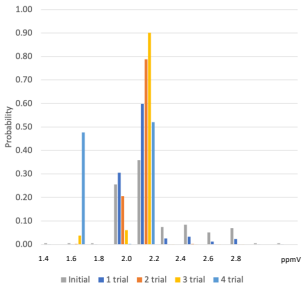

Figure C.2. Illustration of shifting probability distribution informed by local measurements.

J. Houston Miller[2], David Bomse[1], Monica Flores[2], Anthony Gomez[1]

[1] Mesa Photonics, [2]George Washington University,

DoE DE-SC0019543
(Atmospheric Radiation Measurement)